Open Access

OBM Neurobiology

LIDSEN Publishing Inc.

Original Research

Unraveling Bioactive Constituents Isolated from *Knema hookeriana* Warb. as Potential Acetylcholinesterase Inhibitors

Abubakar Siddiq Salihu [1, 2, †], Wan Mohd Nuzul Hakimi Wan Salleh [1, †, *], Nurunajah Ab Ghani [3, 4, †], Mohd Hafiz Arzmi [5, †], Bunleu Sungthong [6, †], Ravikumar Kapavarapu [7, †]

1. Department of Chemistry, Faculty of Science and Mathematics, Universiti Pendidikan Sultan Idris, Tanjong Malim, Perak, Malaysia; E-Mails: asidsal11@gmail.com; wmnhakimi@fsmt.upsi.edu.my
2. Department of Pure and Industrial Chemistry, Faculty of Natural and Applied Science, Umaru Musa Yar'adua University, Katsina, Nigeria
3. Atta-ur-Rahman Institute for Natural Product Discovery (AuRIns), Universiti Teknologi MARA, Bandar Puncak Alam, Selangor, Malaysia; E-Mail: nurunajah@uitm.edu.my
4. Faculty of Applied Sciences, Universiti Teknologi MARA, Shah Alam, Selangor, Malaysia
5. Department of Fundamental Dental and Medical Sciences, Kuliyyah of Dentistry, International Islamic University Malaysia, Kuantan, Pahang, Malaysia; E-Mail: hafizarzmi@iium.edu.my
6. Department of Pharmaceutical Sciences, Faculty of Pharmacy, Mahasarakham University, Maha Sarakham, Thailand; E-Mail: bunleu.s@msu.ac.th
7. Department of Pharmaceutical Chemistry and Phytochemistry, Nirmala College of Pharmacy, Atmakur, Mangalagiri Mandal, Andhra Pradesh, India; E-Mail: ravik4941@gmail.com

† These authors contributed equally to this work.

* **Correspondence:** Wan Mohd Nuzul Hakimi Wan Salleh; E-Mail: wmnhakimi@fsmt.upsi.edu.my

Academic Editor: Talha Bin Emran

Special Issue: Natural Products and Their Bioactive Compounds for Treatment of Neurodegenerative Brain Disorder

OBM Neurobiology
2025, volume 9, issue 2
doi:10.21926/obm.neurobiol.2502286

Received: March 05, 2025
Accepted: April 18, 2025
Published: April 27, 2025

Abstract

The Myristicaceae family, particularly the Knema genus, is renowned for its diverse bioactive compounds, including lignans, flavonoids, and phenolics. This study explores the phytochemical profile of *Knema hookeriana* Warb. leaves and evaluates their potential as acetylcholinesterase (AChE) inhibitors. Phytochemical extraction was performed using a cold maceration method with a polarity-gradient solvent system (hexane, ethyl acetate, and methanol). The isolated compounds were purified through chromatographic techniques and structurally characterized using spectroscopic analyses (IR, NMR, and MS) alongside literature comparison. AChE inhibitory activity was assessed using the Ellman method. Seven bioactive compounds were successfully isolated: aptosimon (1), cubebin acetate (2), bicubebin A (3), 5,7-dimethoxyflavone (4), 4',5,7-trimethoxyflavone (5), luteolin (6), and epicatechin (7). Among these, aptosimon (1) exhibited the most potent AChE inhibition, with an IC_{50} value of 60.8 µg/mL. Molecular docking studies corroborated the in vitro results, demonstrating strong AChE binding affinities for the compounds, with aptosimon (1) showing favorable interactions. These findings highlight the therapeutic potential of *Knema* species and their bioactive compounds, paving the way for further research into their nutraceutical and pharmaceutical applications, particularly in neurodegenerative disease management.

Keywords

Myristicaceae; *Knema hookeriana*; acetylcholinesterase; molecular docking; flavonoid; lignan

1. Introduction

Acetylcholinesterase (AChE) is an essential enzyme that breaks down acetylcholine (ACh) into choline and acetate, thereby regulating cholinergic neurotransmission. This enzymatic process is crucial for normal synaptic function in the central and peripheral nervous systems. However, excessive AChE activity results in rapid acetylcholine degradation, which can impair cognitive function and contribute to neurodegenerative diseases such as Alzheimer's disease (AD) and Parkinson's disease [1, 2]. As a result, AChE inhibitors (AChEIs) have gained significant attention for their potential to enhance cholinergic signaling and improve cognitive function [3]. Synthetic AChE inhibitors, such as donepezil, rivastigmine, and galantamine, are widely used in treating AD. These drugs work by inhibiting AChE, thereby increasing acetylcholine levels and improving memory and cognition. However, their long-term use is often associated with side effects, including nausea, vomiting, diarrhea, and hepatotoxicity. This has led researchers to explore natural AChE inhibitors derived from plants, which may offer safer and more effective alternatives with fewer adverse effects [4].

Phytochemicals, the bioactive compounds found in plants, have demonstrated promising AChE inhibitory properties. Several classes of phytochemicals, including alkaloids, flavonoids, terpenoids, lignans, and phenolics, have been reported to interact with AChE and modulate its activity [3]. Alkaloids such as galantamine and huperzine A are well-known natural AChE inhibitors approved for clinical use [3, 5]. Flavonoids like luteolin, quercetin, and kaempferol exhibit AChE inhibitory effects and neuroprotective benefits due to their antioxidant and anti-inflammatory properties. Similarly,

terpenoids, including ginkgolides have been shown to enhance cognitive function by modulating neurotransmitter activity [6]. Lignans, another important class of phytochemicals, are increasingly being studied for their potential AChE inhibitory activity. Neolignans and other lignan derivatives, found in medicinal plants such as *Knema* species, have demonstrated promising neuroprotective effects [7]. Phenolic compounds, including tannins and phenolic acids, have also been shown to inhibit AChE through interactions with the enzyme's active and peripheral binding sites [8]. These findings highlight the diverse chemical structures of plant-derived AChE inhibitors and their potential therapeutic applications in neurodegenerative disorders.

In recent years, molecular docking studies have played a crucial role in the discovery and characterization of AChE inhibitors from natural sources. Computational approaches such as molecular docking and molecular dynamics simulations allow researchers to predict the binding affinity, interaction sites, and inhibitory mechanisms of phytochemicals against AChE. These in silico studies provide valuable insights into the structure-activity relationships (SARs) of plant-derived compounds, guiding further experimental validation through in vitro and in vivo assays [9].

Despite the promising potential of plant-derived AChE inhibitors, several challenges remain. Bioavailability, pharmacokinetics, and large-scale production must be addressed before these compounds can be developed into viable drugs. Future research should focus on optimizing the formulation and delivery of phytochemicals to enhance their therapeutic efficacy. Additionally, integrating computational studies with experimental approaches will be crucial in advancing phytochemical-based drug discovery [10]. Hence, phytochemicals offer a natural and potentially safer alternative to synthetic AChE inhibitors. The continued exploration of plant-derived bioactive compounds, particularly from the genus *Knema*, may lead to the discovery of novel AChE inhibitors with improved safety and efficacy profiles.

The Myristicaceae family, a uniform group within the Magnoliales order, includes 23 genera and 520 species. Many species in this family are known for their traditional and medicinal applications in Southeast Asia, particularly Malaysia and Indonesia [7]. The *Knema* genus is notably the third-largest genus within the Asian Myristicaceae, comprising around sixty species in Southeast Asia. Several *Knema* species are used in traditional medicine to address conditions like tumors, skin irritation, wounds, inflammation, and digestive disorders.[8] Limited studies on the phytochemistry of the *Knema* genus indicate the presence of various bioactive compounds such as alkyl and acyl resorcinol derivatives of phenylalkylphenol, flavonoids, lignans, and stilbenes. These compounds have demonstrated significant acetylcholinesterase inhibitory, cytotoxic, anti-inflammatory, nematicidal, and antibacterial activities [9].

Knema hookeriana Warb., a tree species native to Indonesia, Malaysia, Singapore, and Thailand, grows to a height of 15-20 meters with a trunk diameter of up to 50 cm. Its leaves are simple and opposite, measuring 7-15 cm in length and 5-8 cm in width [10]. Traditionally, this plant has been used to treat stomach aches, and its sap is utilized for dyeing nets and fabrics. Additionally, it serves as a surface coating for preserving wooden, porcelain, and metallic items [11]. Research on *K. hookeriana* has been limited, with only three studies investigating its anti-cholinesterase, anti-nematodal, and anti-apoptotic properties. Phytochemical analyses have identified the presence of acetophenones, anacardic acid, and cardanols [12]. Recently, we managed to report the chemical composition, acetylcholinesterase inhibition and molecular docking studies of essential oil from this species [13]. Given the documented acetylcholinesterase inhibitory activity of essential oils from *K.*

hookeriana, it is hypothesized that the leaf extracts of this species contain bioactive compounds capable of inhibiting AChE.

As a continuation study of this species, this study aims to assess the acetylcholinesterase inhibitory activity of the isolated compounds from *K. hookeriana* leaf extracts against the acetylcholinesterase enzyme. Furthermore, a molecular docking study was also conducted on the isolated phytochemicals to explore their interactions with AChE-associated proteins and provide insights into their potential mechanisms of action.

2. Materials and Methods

2.1 Plant Material

The leaves of *K. hookeriana* were collected from Behrang, Perak (with latitude 3°44'51.612''N and longitude 101°27'19.9008''E at an elevation of 52 m above sea level) in October 2019 and identified by a botanist, Dr. Shamsul Khamis from Universiti Kebangsaan Malaysia (UKM). The voucher specimens (SK29/19) have been deposited at the UKMB Herbarium, UKM.

2.2 General Experimental Procedures

The cold extraction method was used to obtain the crude extract from the dried samples using n-hexane, EtOAc, and MeOH, which yielded crude extracts in sufficient quantities for subsequent chromatographic separation and spectroscopic analysis. Gravity column chromatography (CC) was performed using Merck SiO_2 (70-230 Mesh). Thin layer chromatography (TLC) analysis was conducted on 0.20 mm precoated silica gel aluminum sheets (Merck Kieselgel 60 F_{254}). Preparative thin layer chromatography (PTLC) was carried out using 1 mm thin glass plates of Merck SiO_2 60 F_{254}. N-Hexane, EtOAc, DCM, $CHCl_3$, Et_2O, and MeOH were used as solvent systems in chromatographic methods. The spots on the TLC plate were detected under ultraviolet (UV) illumination at 254 nm and 365 nm, followed by spraying with vanillin-sulfuric acid reagent. All reagents used in this study were analytical and purchased from Sigma Aldrich. For structural elucidation, Infrared (IR) Spectroscopy, Nuclear Magnetic Resonance (NMR) Spectroscopy, and Mass Spectrometry (MS) analyses were performed. The IR spectrum was recorded using a Perkin Elmer Series 1600 spectrophotometer (KBr pellet for solid and NaCl discs for liquid samples) and a Perkin Elmer Spectrum 100 FT-IR Spectrometer. 1D and 2D NMR spectra were obtained using a JEOL Spectrometer (JNM-ECX-500), with chemical shifts reported in ppm. Residual solvents ($CDCl_3$ and MeOD) served as internal standards. Mass spectral data were acquired using Liquid Chromatography Mass Spectrometry (Exactive, Thermo Fisher Scientific).

2.3 Extraction and Isolation

The crude extracts of n-hexane (12.6 g, 1.3%), EtOAc (32.7 g, 3.3%), and MeOH (33.8 g, 3.4%) were produced. While the *n*-hexane extract was subjected to chromatography, it did not yield any isolable pure compounds and was not pursued further. In contrast, the crude EtOAc extract (KHLE) was chromatographed using a solvent system of n hexane:$CHCl_3$:EtOAc, affording seventeen fractions that were subsequently pooled based on their appearance, Rf values, and TLC profiles. Purification of fraction KHLE A6 provided compound **(1)** (126 mg), while further processing of fractions KHLE A7 and KHLE A11 yielded compound **(2)** (56 mg) and compound **(3)** (33 mg),

respectively. Meanwhile, the crude MeOH extract (KHLM), enriched with more polar constituents was subjected to CC using an eluent system of n hexane:$CHCl_3$:EtOAc:methanol. This procedure yielded several fractions, which were pooled based on TLC analysis, and further purified to afford compound **(4)** (87 mg) from fraction KHLM B3, compound **(5)** (100 mg) from fraction KHLM B4, compound **(6)** (77 mg) from fraction KHLM B5, and compound **(7)** (61 mg) from fraction KHLM B6.

2.4 Spectral Data

Aptosimon (1): colorless crystalline solid (120.0 mg). ^{1}H NMR ($CDCl_3$, 500 MHz): δ 3.52 (1H, m, H-1), 5.26 (1H, d, J = 1.8 Hz, H-2), 3.44 (1H, dd, J = 8.1, 2.8 Hz, H-5), 5.70 (1H, d, J = 1.8 Hz, H-6), 3.85 (1H, d, J = 4.3 Hz, H-8a), 3.50 (1H, dd, J = 7.5, 4.3 Hz, H-8b), 6.85 (1H, s, H-2′), 6.83 (1H, m, H-5′), 6.85 (1H, m, H-6′), 5.95 (2H, s, H-7′), 6.96 (1H, s, H-2′′), 6.77 (1H, m, H-5′′), 6.77 (1H, m, H-6′′), 5.99 (2H, s, H-7′′). ^{13}C NMR ($CDCl_3$, 125 MHz): δ 45.4 (C-1), 83.6 (C-2), 176.7 (C-4), 54.8 (C-5), 80.1 (C-6), 68.6 (C-8a/8b), 134.5 (C-1′), 108.3 (C-2′), 148.1 (C-3′), 148.0 (C-4′), 106.0 (C-5′), 118.9 (C-6′), 101.3 (C-7′), 129.7 (C-1′′), 108.5 (C-2′′), 147.5 (C-3′′), 147.3 (C-4′′), 105.5 (C-5′′), 118.2 (C-6′′), 101.1 (C-7′′). MS *m/z* 391.28 $[M + Na]^+$, $C_{20}H_{16}O_6$ [14].

Cubebin Acetate (2): Colorless crystalline solids (112 mg). ^{1}H NMR ($CDCl_3$, 500 MHz): δ 6.67–6.62 (1H, m, H-2, H-5, H-6), 6.41–6.32 (1H, m, H-2′, H-5′, H-6′), 2.35 (2H, m, H-7), 2.04 (1H, m, H-8), 5.37 (1H, d, J = 10.1 Hz, H-9), 2.37 (2H, m, H-7′), 2.39 (1H, m, H-8′), 3.82 (1H, t, J = 8.2 Hz, H-9′), 3.99 (1H, t, J = 8.2 Hz, H-9′), 2.06 (1H, s, H-11), 5.94 (4H, s, OCH_2O). ^{13}C NMR ($CDCl_3$, 125 MHz): δ 133.6 (C-1), 108.8 (C-2), 148.0 (C-3), 147.5 (C-4), 107.9 (C-5), 121.2 (C-6), 39.2 (C-7), 56.6 (C-8), 76.3 (C-9), 132.2 (C-1′), 107.3 (C-2′), 147.8 (C-3′), 145.8 (C-4′), 108.0 (C-5′), 121.3 (C-6′), 40.5 (C-7′), 42.99 (C-8′), 72.0 (C-9′), 21.1 (C-11), 170.0 (C=O), 100.1 (OCH_2O). MS *m/z* 414.41 $[M]^+$, $C_{22}H_{22}O_8$ [15].

Bicubebin A (3): White solid (56.0 mg). ^{1}H NMR ($CDCl_3$, 500 MHz): δ 6.59 (1H, d, J = 1.5 Hz, H-2), 6.77–6.61 (1H, m, H-5), 6.77–6.61 (1H, m, H-6), 2.33 (1H, m, H-7), 2.53 (1H, m, H-7), 2.02–2.21 (1H, m, H-8), 5.24 (1H, d, J = 1.4 Hz, H-9); 6.50–6.59 (1H, m, H-2′), 6.61 (1H, d, J = 7.9 Hz, H-5′), 6.50–6.59 (1H, m, H-6′), 2.56 (1H, m, H-7′), 2.73 (1H, m, H-7′), 2.01–2.20 (1H, m, H-8′), 4.13 (1H, t, J = 8.3 Hz, H-9′), 3.93 (1H, t, J = 8.3 Hz, H-9′), 3.63 (1H, t, J = 8.4, 7.8 Hz, H-9′); 6.77–6.61 (1H, m, H-2′′), 6.77–6.61 (1H, m, H-5′′), 6.77–6.61 (1H, m, H-6′′), 2.36 (1H, m, H-7′′), 2.53 (1H, m, H-7′′), 2.02–2.21 (1H, m, H-8′′), 5.15 (1H, d, J = 1.4 Hz, H-9′′); 6.39–6.42 (1H, m, H-2′′′), 6.60 (1H, d, J = 7.9 Hz, H-5′′′), 6.50–6.59 (1H, m, H-6′′′), 2.56 (1H, m, H-7′′′) 2.73 (1H, m, H-7′′′), 2.01–2.20 (1H, m, H-8′′′), 4.03 (1H, t, J = 8.3 Hz, H-9′′′), 3.81 (1H, t, J = 8.4, 7.8 Hz, H-9′′′), 3.40 (1H, t, J = 8.4, 7.8 Hz, H-9′′′), 5.95 (8H, s, 4 × OCH_2O). ^{13}C NMR ($CDCl_3$, 125 MHz): δ 133.5 (C-1), 108.9 (C-2), 147.6 (C-3), 145.9 (C-4), 108.1 (C-5), 121.8 (C-6), 38.3 (C-7), 52.6 (C-8), 103.4 (C-9); 134.2 (C-1′), 108.8 (C-2′), 147.7 (C-3′), 145.8 (C-4′), 108.2 (C-5′), 121.2 (C-6′), 39.2 (C-7′), 45.7 (C-8′), 72.0 (C-9′); 133.3 (C-1′′), 109.2 (C-2′′), 147.7 (C-3′′), 145.7 (C-4′′), 108.0 (C-5′′), 121.3 (C-6′′), 39.0 (C-7′′), 52.3 (C-8′′), 104.2 (C-9′′); 134.5 (C-1′′′), 109.3 (C-2′′′), 147.5 (C-3′′′), 145.7 (C-4′′′), 108.6 (C-5′′′), 121.6 (C-6′′′), 33.6 (C-7′′′), 43.5 (C-8′′′), 72.5 (C-9′′′), 100.8 (4 × OCH_2O). MS *m/z* 729.219 $[M + Cl]^-$, $C_{40}H_{38}O_{11}$ [16].

5,7-Dimethoxyflavone (4): White solid (33.3 mg). ^{1}H NMR ($CDCl_3$, 500 MHz): δ 3.99 (3H, s, 5-OCH_3); 3.95 (3H, s, 7-OCH_3); 6.83 (1H, s, H-3); 6.62 (1H, d, J = 2.2 Hz, H-6); 6.42 (1H, d, J = 2.2 Hz, H-8); 7.53 (3H, m, H-3′, H-4′, H-5′); 7.92 (2H, m, H-2′/H-6′). ^{13}C NMR ($CDCl_3$, 125 MHz): δ 107.9 (C-4a); 131.7 (C-1′); 160.1 (C-2); 161.0 (C-7); 160.1 (C-5); 164.8 (C-8a); 177.8 (C-4); 92.8 (C-6); 96.6 (C-8); 107.9 (C-3); 126.2 (C-2′/C-6′); 129.0 (C-3′/C-5′); 131.0 (C-4′); 56.5 (7-OCH_3); 55.9 (5-OCH_3). MS *m/z* 283.11 $[M + H]^+$, $C_{17}H_{14}O_4$ [17].

4',5,7-Trimethoxyflavone (5): Yellow crystalline needles (87.0 mg). ^{1}H NMR ($CDCl_3$, 500 MHz): δ 6.69 (1H, s, H-3); 6.57 (1H, d, J = 2.1 Hz, H-6); 6.37 (1H, d, J = 2.1 Hz, H-8); 7.84 (1H, d, J = 9.0 Hz, H-2'); 7.00 (1H, d, J = 9.0 Hz, H-3'); 7.00 (1H, d, J = 9.0 Hz, H-5'); 7.84 (1H, d, J = 9.0 Hz, H-6'); 3.95 (3H, s, 5-OCH_3); 3.91 (3H, s, 7-OCH_3); 3.88 (3H, s, 4'-OCH_3). ^{13}C NMR ($CDCl_3$, 125 MHz): δ 162.1 (C-2); 107.7 (C-3); 177.7 (C-4); 109.2 (C-4a); 160.9 (C-5); 92.3 (C-6); 163.9 (C-7); 96.1 (C-8); 159.8 (C-8a); 123.9 (C-1'); 127.6 (C-2'); 114.4 (C-3'); 159.8 (C-4'); 114.4 (C-5'); 127.6 (C-6'); 55.5 (5-OCH_3); 55.7 (7-OCH_3); 56.3 (4'-OCH_3). MS *m/z* 313.107 $[M + H]^+$, $C_{18}H_{16}O_5$ [18].

Luteolin (6): White solid (61.0 mg). ^{1}H NMR ($CDCl_3$, 500 MHz): δ 6.47 (1H, s, H-3); 5.99 (1H, d, J = 2.0 Hz, H-8); 6.24 (1H, d, J = 2.0 Hz, H-6); 7.31 (1H, d, J = 2.3 Hz, H-6'); 6.73 (1H, d, J = 8.1 Hz, H-6'); 7.28 (1H, dd, J = 8.1, 2.3 Hz, H-5'). ^{13}C NMR ($CDCl_3$, 125 MHz): δ 164.1 (C-2); 102.3 (C-3); 181.5 (C-4); 102.8 (C-4a); 161.8 (C-5); 100.1 (C-6); 161.8 (C-7); 94.8 (C-8); 158.0 (C-8a); 120.4 (C-1'); 112.8 (C-2'); 146.9 (C-3'); 152.4 (C-4'); 116.3 (C-5'); 119.4 (C-6'). MS *m/z* 285.45 $[M]^+$, $C_{15}H_{14}O_6$ [19].

Epicatechin (7): Yellow solid (77.0 mg). ^{1}H NMR ($CDCl_3$, 500 MHz): δ 4.62 (1H, d, J = 7.5 Hz, H-2), 3.96 (1H, m, H-3), 2.41 (2H, dd, J = 15.9, 8.4 Hz, H-4), 2.65 (2H, dd, J = 15.9, 5.4 Hz, H-4), 5.85 (1H, d, J = 1.8 Hz, H-6), 5.67 (1H, d, J = 1.8 Hz, H-8), 6.85 (1H, d, J = 1.5 Hz, H-2'), 6.61 (1H, d, J = 8.2 Hz, H-5'), 6.62 (1H, d, J = 8.2 Hz, H-6'), 9.07 (1H, s, 5-OH), 8.85 (1H, s, 7-OH), 8.68 (1H, s, 3'-OH), 8.76 (1H, s, 4'-OH). ^{13}C NMR ($CDCl_3$, 125 MHz): δ 78.5 (C-2), 65.4 (C-3), 28.7 (C-4), 156.3 (C-5), 94.6 (C-6), 156.7 (C-7), 95.5 (C-8), 157.0 (C-9), 99.0 (C-10), 131.1 (C-1'), 115.2 (C-2'), 145.0 (C-3'), 144.9 (C-4'), 115.3 (C-5'), 118.4 (C-6'). MS *m/z* 219.20 $[M + H]^+$, $C_{15}H_{14}O_6$ [20].

2.5 Acetylcholinesterase (AChE) Inhibitory Activity

The isolated compounds were evaluated for their acetylcholinesterase activity by assessing their AChE inhibitory effects. The spectrophotometric method was used with modifications [21-23]. AChE from *Electrophorus electricus* and acetylthiocholine iodide were used as substrates. The acetylcholinesterase activity was determined using 5,5'-dithiobis (2-nitrobenzoic acid) (DTNB). In brief, a 96-well microplate was used to combine 140 µL of sodium phosphate buffer (pH 8.0), 20 µL of DTNB, 20 µL of compounds (at final concentrations of 5, 10, 25, 50, and 100 µM), and 20 µL of AChE (0.22 U/mL) solution. This mixture was incubated at 25°C for 15 min before adding 10 µL of acetylthiocholine iodide to initiate the reaction. The hydrolysis of acetylthiocholine iodide was measured by monitoring the formation of the yellow 5-thio-2-nitrobenzoate anion at 412 nm using a 96-well microplate reader (Epoch Micro-Volume Spectrophotometer, USA). Ethanol (EtOH) was used to dissolve the test compounds, and a blank sample containing only EtOH in phosphate buffer (without compounds) served as the solvent control to correct for any effect of the solvent on enzyme activity. The inhibition percentage (I%) of AChE was calculated by comparing the reaction rates relative to the blank sample using the formula: I% = [E - S/E] × 100; where E is the enzyme activity without the test sample and S is the enzyme activity with the test sample. All tests were carried out in triplicate, and IC_{50} values were reported as means ± SD of triplicate. Galantamine was used as positive control at Galantamine was used as a positive control at concentrations of 0.5, 1.0, and 2.0 µM.

2.6 Molecular Docking and Toxicity Studies

The crystal structure of acetylcholinesterase (AChE) from *Electrophorus electricus* (PDB ID: 1C2O) [24] was retrieved from the RCSB Protein Data Bank (https://www.rcsb.org/). Hydrogen atoms were

added into the enzyme structure using Biovia Discovery Studio [25]. A grid box was constructed to encompass the entirety of the "active site gorge," which includes the catalytic triad (S203, E334, and H447) as well as other crucial regions, as shown in Figure 1 [26]. The grid box was constructed using AutoDockTools, with dimensions of 20 Å × 20 Å × 20 Å and a grid spacing of 1 Å.

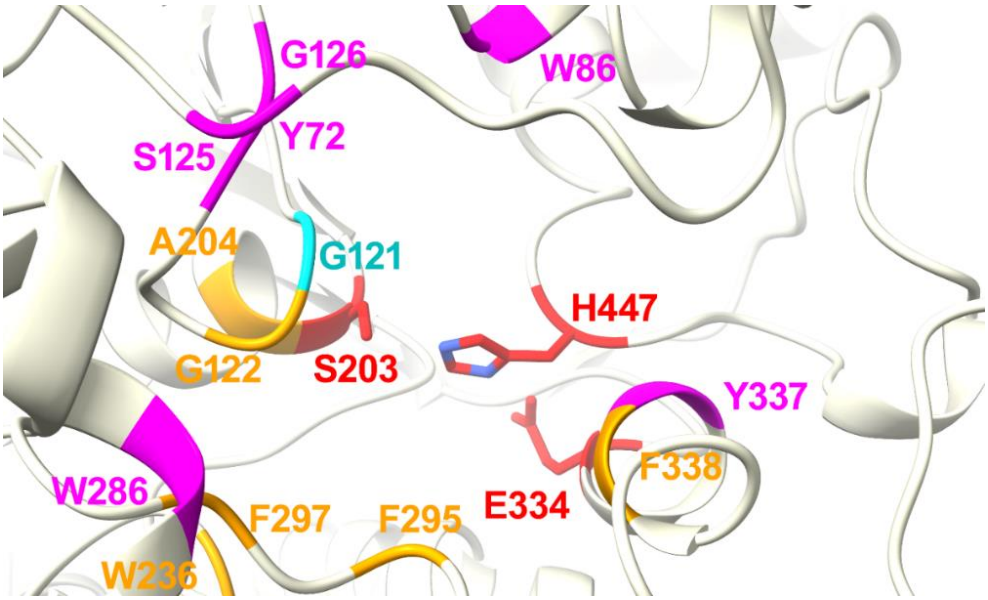

Figure 1 Catalytic triads (red) and crucial regions of AChE of Electrophorus electricus: peripheral anionic binding site (PAS) (Magenta), oxyanion hole (OAH) (Cyan), and acyl binding site (ABS) (Orange).

The 3D structures of all isolated compounds were generated using GaussView 03 [27], followed by energy minimization employing the semi-empirical Polak-Ribiere method using conjugate gradients. These structures were subsequently converted into.pdb format using Biovia Discovery Studio. A grid box, centered around the catalytic triad, was set up based on the docking validation parameters using AutoGrid 4.2. The docking calculations were performed using AutoDock 4.2 [28], wherein the enzyme was treated as rigid, while the ligand was allowed to move freely [29]. The resulting protein-ligand complexes were visualized using Discovery Studio and Chimera X [25, 30]. Toxicity predictions were performed using the latest ProTox 3.0 platform, available at https://tox.charite.de, which uses molecular similarity and machine learning to estimate multiple toxicity endpoints [31].

3. Results and Discussion

Seven compounds (Figure 2) were successfully isolated from the leaf extract of *K. hookeriana*. These compounds were identified as a furofuran lignan; aptosimon **(1)** as well as two other cubebin typed lignan; cubebin acetate **(2)** and bicubebin A **(3)**. In addition, two known methoxyflavones and a hydroxyflavone were also identified, which are 5,7-dimethoxyflavone **(4)** and 4',5,7-trimethoxyflavone **(5)**, and luteolin **(6)** respectively. In addition, a flavonol; epicatechin **(7)** was also isolated. These compounds' characterization and structural elucidations were established by extensive spectroscopic data analysis and comparison with literature data [14-20, 32-36].

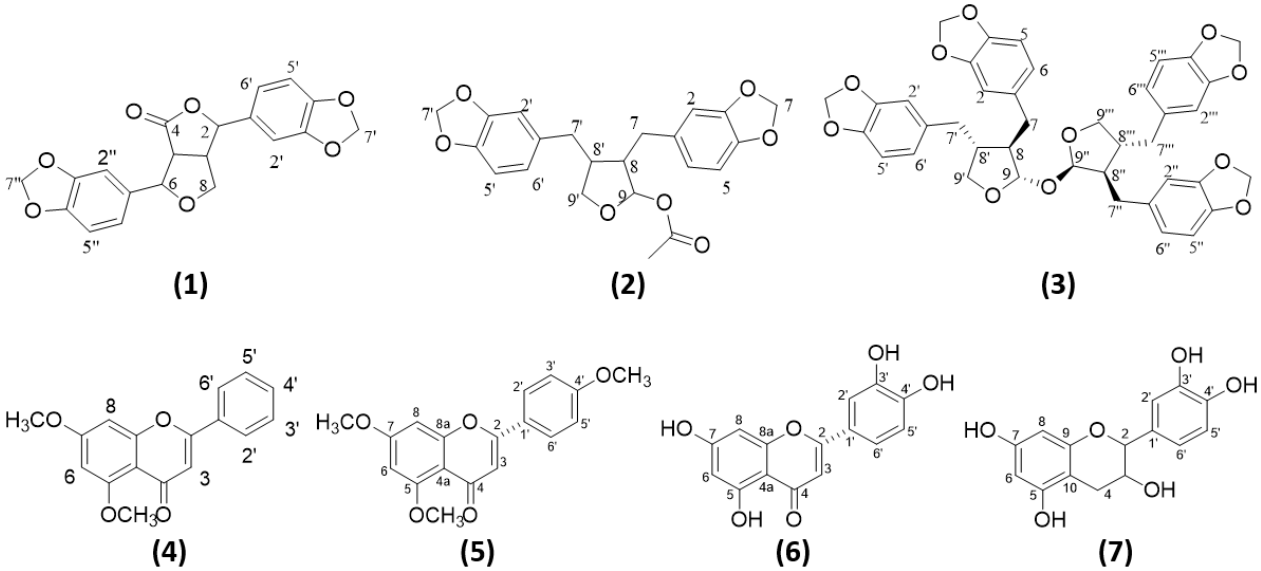

Figure 2 Chemical structures of isolated compounds from *K. hookeriana*.

Compound **(1)** was isolated from the EtOAc extract as a colorless crystalline solid. The ^{1}H NMR spectrum displayed signals consistent with a lignan structure. A multiplet at δ 3.52 integrated for one proton was assigned to a methine proton (H-1) adjacent to an oxygen-bearing carbon. The doublet at δ 5.26 (J = 1.8 Hz) was attributed to the methine proton (H-2) on the furan ring. The methine protons at positions C-5 and C-6 appeared as a doublet of doublets at δ 3.44 (J = 8.1 and 2.8 Hz) and a doublet at δ 5.70 (J = 1.8 Hz), respectively, indicating ether groups. Besides, two methylene protons (H-8a and H-8b) were observed at δ 3.85 (J = 4.3 Hz) and 3.55 (J = 7.5 and 4.3 Hz), corresponding to methylene groups adjacent to aromatic rings. The aromatic region of the spectrum revealed protons resonating between δ 6.77 (H-5"/H-6") and 6.96 (H-2"), consistent with a conjugated aromatic system. In addition, singlet protons at δ 5.95 and 5.98 were attributed to methylenedioxy groups on aromatic rings. The ^{13}C NMR spectrum confirmed the presence of 24 carbon atoms. Key signals included δ 176.7 for the ester carbonyl carbon (C-4), δ 83.6 and 80.1 for oxygenated methine carbons (C-2 and C-6), and δ 45.4 for the methine carbon (C-1). Aromatic carbons resonated between δ 105.5 (C-5") and 148.1 (C-3'), while the methylene carbons appeared at δ 68.6 (C-8). In addition, the methylenedioxy carbons were observed at δ 101.1 and 101.3.

Compound **(2)** was isolated as a colorless crystalline solid from the MeOH extract. The ^{1}H NMR spectrum displayed multiplets signal for aromatic protons at δ 6.67–6.62 (H-2, H-5, H-6) and δ 6.41–6.32 (H-2′, H-5′, H-6′), consistent with two aromatic rings. Signals for benzylic methylene protons (H-7, H-7′) were observed at δ 2.35 and δ 2.37, while signals at δ 2.04 (H-8) and 2.39 (H-8′) corresponded to adjacent methylene groups. The methine proton of the hemiacetal group (H-9) resonated as a doublet at δ 5.37 (J = 10.1 Hz). In contrast, the diastereotopic protons of the methyleneoxy group (H-9′) appeared as a triplet at δ 3.82 (J = 8.2 Hz) and 3.99 (J = 8.2 Hz). Additionally, a singlet at δ 2.06 was attributed to the acetate methyl group (C-11). The ^{13}C NMR spectrum confirmed the presence of 22 carbon atoms, including two methyleneoxy carbons (δ 100.1), aromatic carbons (δ 107.3–148.0), and a carbonyl carbon of the acetate group (δ 170.0). The benzylic carbons (C-7/C-7′) resonated at δ 39.2 and 40.5, while the carbons for the methyleneoxy protons (C-9′) appeared at δ 72.0.

Compound **(3)** was isolated as a white solid from the EtOAc extract. It represents a lignan-type molecule with a symmetrical dicubebin framework, characterized by its methylenedioxy and aromatic substitution patterns. The ^{1}H NMR spectrum provided detailed insights into its proton environment. The aromatic protons appeared as multiplets between δ 6.50–6.59 (H-2'), with a prominent doublet at δ 6.59 (J = 1.5 Hz) assigned to H-2. The multiplet signals at δ 6.61–6.77 corresponded to H-5 and H-6, confirming a substituted aromatic ring. The B-ring protons mirrored these patterns, reflecting the compound's symmetrical structure. In the aliphatic region, multiplet signals at δ 2.33 and 2.53 were attributed to H-7, while another broad multiplet at δ 2.02–2.21 corresponds to H-8. The oxygenated methine proton at δ 5.24 (d, J = 1.4 Hz) was characteristic of H-9, the other methine proton at δ 5.15 (d, J = 1.4 Hz) was characteristic of H-9'', indicative of the ether bridge connecting the two cubebin units. The methylenedioxy protons were observed as singlets at δ 5.95, correlating to their attachment to aromatic carbons. The ^{13}C NMR spectrum revealed 40 carbon signals, consistent with the symmetrical dicubebin framework. The aromatic carbons displayed characteristic shifts between δ 133.5 (C-1) and 147.7 (C-3'), with δ 108.0 (C-5'') and 108.9 (C-2) assigned to carbons directly bonded to methylenedioxy groups. The methylenedioxy carbons appeared at δ 100.8, confirming their presence in the structure. Besides, the oxygenated methine carbons (C-9) resonated at δ 103.4, while the methylene carbons were observed at δ 38.3 (C-7) and 52.6 (C-8), respectively.

Compound **(4)** afforded a white crystalline solid from EtOAc extract. The ^{1}H NMR spectrum showed two singlet signals at δ 3.99 and 3.95, corresponding to methoxyl groups at positions C-5 and C-7, respectively. A singlet signal at δ 6.83 was attributed to H-3. Two meta-coupled doublets at δ 6.42 and 6.62 (J = 2.2 Hz) corresponded to H-8 and H-6 of ring A, respectively. The aromatic protons of ring B appeared as a multiplet at δ 7.53 (three protons, H-3', H-4', and H-5') and δ 7.92 (H-2'/H-6'). The ^{13}C NMR spectrum confirmed the presence of 17 carbon atoms. The DEPT spectrum further classified them into seven quaternary carbons, eight methine carbons, and two methoxy carbons.

Compound **(5)** was isolated as yellow crystalline needles from the MeOH extract. The ^{1}H NMR spectrum closely resembled the ^{1}H NMR spectrum of compound **(4)** except for three methoxyl groups at δ 3.95, 3.91, and 3.88. Instead of a monosubstituted aromatic signal, this compound displayed signals for a para-disubstituted moiety. These signals were observed at δ 7.00 and 7.84 (2H, d, J = 9.0 Hz) attributed to H-3'/H-5' and H-2'/H-6' of ring B of a flavonoid system. The ^{13}C NMR spectrum showed the presence of eighteen signals attributed to eighteen carbons. The spectrum was similar to compound **(4)** with an additional primary carbon at C-4' (δ 56.3) attributed to a methoxyl carbon. The DEPT spectrum provided a clear differentiation between protonated and quaternary carbons. The methoxy carbons and the C-3 proton were confirmed as CH_3 and CH groups, respectively, while the absence of proton signals on the substituted carbons validated the placement of methoxy groups.

Compound **(6)** was obtained as a white solid from the MeOH extract. The ^{1}H NMR spectrum displayed well-defined proton signals consistent with the flavonoid framework. On the A-ring, two doubles at δ 5.99 (1H, d, J = 2.0 Hz, H-6) and 6.24 (1H, d, J = 2.0 Hz, H-8) represented meta-coupled aromatic protons. The chemical shifts of these protons were slightly downfield due to the influence of the hydroxyl group at C-5 and the conjugated carbonyl group at C-4. The singlet at δ 6.47 corresponded to H-3, located within the pyranone ring. In addition, for the B-ring, the ABX spin system was evident, with δ 7.31 (d, J = 2.3 Hz, H-2'), 6.73 (d, J = 8.1 Hz, H-5'), and 7.28 (dd, J = 8.1,

2.3 Hz, H-6'). This splitting pattern indicated ortho and meta couplings consistent with the substitution pattern of hydroxyl groups at C-3' and C-4'. The ^{13}C NMR spectrum revealed the presence of 15 distinct carbon resonances, which were categorized as one carbonyl carbon, six methine carbons, and eight quaternary carbons, consistent with the flavonoid structure.

Compound **(7)** was isolated as a yellow solid from the MeOH extract. The ^{1}H NMR spectrum revealed a distinctive set of signals corresponding to aliphatic and aromatic protons. In the aliphatic region, H-4 protons appeared as a pair of double doublets at δ 2.41 (J = 15.9, 8.4 Hz, H-4a) and δ 2.65 (J = 15.9, 5.4 Hz, H-4b), confirming the presence of a methylene group adjacent to the C-3 hydroxyl group. The methine proton H-3 resonated at δ 3.96 as a multiplet, consistent with its location in the heterocyclic ring. Another methine proton, H-2 appeared as a doublet at δ 4.62 (J = 7.5 Hz), suggesting its attachment to a hydroxylated chiral center. In the aromatic region, H-6 and H-8 protons from the A-ring resonated as doublets at δ 5.85 (J = 1.8 Hz) and δ 5.67 (J = 1.8 Hz), respectively. Their meta-coupling pattern confirmed their positions on the A-ring, flanked by hydroxylated quaternary carbons. The B-ring protons exhibited a characteristic ABX coupling system, with H-5' appearing at δ 6.61 (J = 8.2 Hz), H-6' at δ 6.62 (J = 8.2 Hz), and H-2' at δ 6.85 (J = 1.5 Hz), all observed as doublets. These patterns corroborate the 1,3,4-trihydroxylated substitution on the B-ring. The ^{13}C NMR spectrum revealed 15 distinct carbon signals, displaying characteristic signals for aromatic, aliphatic, and oxygenated carbons typical of flavan-3-ol derivatives.

The tested compounds showed moderate to weak AChE inhibition, with an IC_{50} value of 60.8 to 102.9 µM. Galantamine, a well-established AChE inhibitor, exhibited an IC_{50} value of 0.5 µM. The results are shown in **Table 1**. Among the tested compounds, aptosimon **(1)** displayed the strongest AChE inhibition with an IC_{50} value of 60.8 µM. In addition, 4',5,7-trimethoxyflavone **(5)** displayed convincing AChE inhibition with an IC_{50} value of 69.2 µM, followed by 5,7-dimethoxyflavone **(4)** (IC_{50} value of 78.4 µM). The relatively higher activity of compound **5** compared to **4** suggests that additional methoxy substitution at the 4' position enhances AChE inhibition, possibly due to increased lipophilicity and better interaction with the enzyme's active site. Bicubebin A **(3)** (IC_{50} value of 85.2 µM) and luteolin **(6)** (IC_{50} value of 89.5 µM) exhibited moderate inhibition, while epicatechin **(7)** (IC_{50} value of 95.6 µM) and cubebin acetate **(2)** (IC_{50} value of 102.9 µM) showed weaker activity. The lower potency of these compounds could be attributed to structural features that may limit their binding efficiency to the AChE active site. Galantamine, a well-established AChE inhibitor, exhibited significantly higher potency (IC_{50} value of 0.5 µM) than all the tested compounds. This dramatic difference highlights the need for further structural modifications to enhance the AChE inhibitory activity of flavones and lignans. Although compounds **1, 4** and **5** showed relatively better inhibition among the tested molecules, they are still far less potent than galantamine, indicating that additional optimization is necessary for therapeutic applications.

Table 1 Acetylcholinesterase activity of isolated compounds.

Compounds	**IC_{50} value (μM)**
Aptosimon **(1)**	60.8
Cubebin acetate **(2)**	102.9
Bicubebin A **(3)**	85.2
5,7-Dimethoxyflavone **(4)**	78.4
4',5,7-Trimethoxyflavone **(5)**	69.2
Luteolin **(6)**	99.5
Epicatechin **(7)**	95.6
Galantamine	0.5

Molecular docking studies provide insight into the binding affinity of various compounds toward AChE, with more negative binding energies (kcal/mol) indicating stronger interactions. **Table 2** shows the docking scores of isolated compounds and the reference inhibitor. Molecular docking analysis was conducted to gain insight into the binding interactions of the isolated compounds with acetylcholinesterase (AChE). The docking scores, which reflect the binding free energy, ranged from -8.0 to -10.2 kcal/mol, indicating favorable ligand-protein interactions (**Table 3**).

Table 2 Docking scores of isolated compounds and reference inhibitors.

Compounds	**AChE (kcal/mol)**
Aptosimon **(1)**	-9.4
Cubebin acetate **(2)**	-10.2
Bicubebin A **(3)**	-10.0
5,7-Dimethoxyflavone **(4)**	-8.7
4',5,7-Trimethoxyflavone **(5)**	-8.5
Luteolin **(6)**	-9.2
Epicatechin **(7)**	-8.0
Galantamine	-7.8

Table 3 Docking scores and critical protein-ligand interactions between AChE and compounds.

Compounds	AChE (kcal/mol)	Hydrogen bond	Van der Waals	Pi-Pi	Pi-Alkyl	3D structure	2D structure
Aptosimon **(1)**	-9.4	Y337, F295, R296	D74, G121, S125, F297, S293, I294, L289, G342	Y124, Y342	Y72, W286	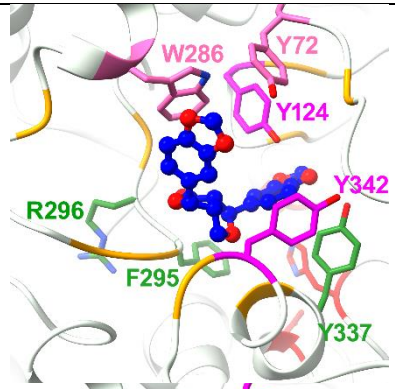	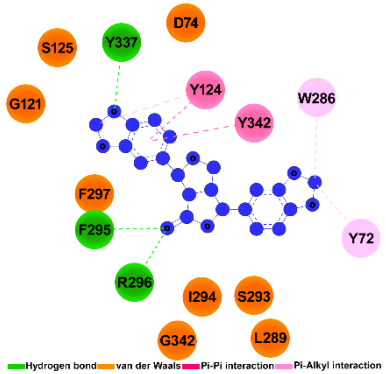
Cubebin acetate **(2)**	-10.2	F295	D74, W86, G120, G121, G122, Y124, E202, S203, L289, S293, I294, F338, Y341, G448	Y72, W286, Y337	H447	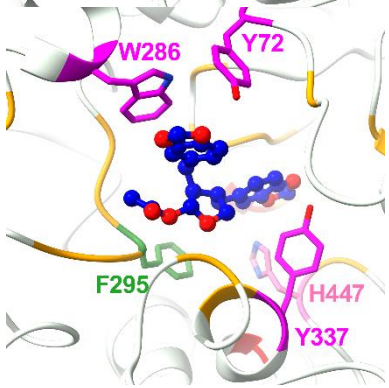	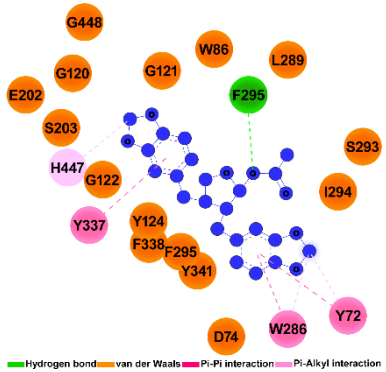

Bicubebin A **(3)**	-10.0	F295	Y72, D74, L76, G121, G122, S125, S293, I294, F295, F338, V340, G342	R124, W286, R341	L289	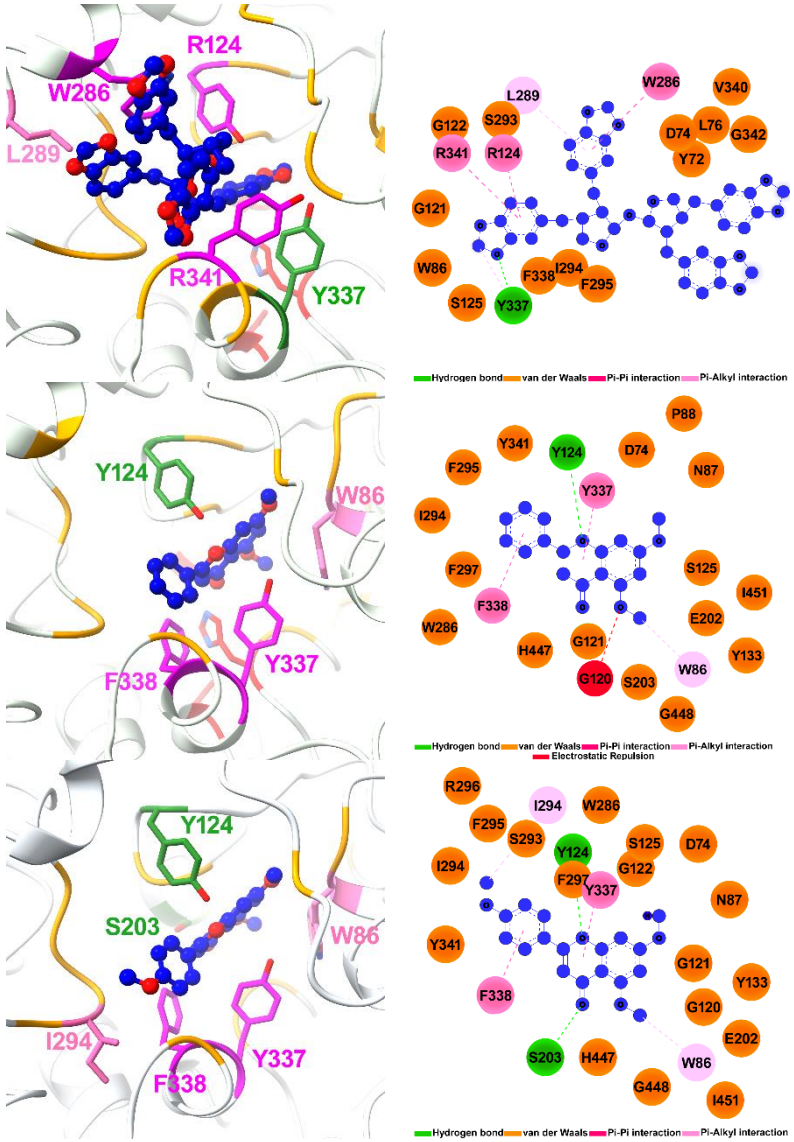
5,7-Dimethoxyflavone **(4)**	-8.7	Y124	D74, N87, P88, G121, S125, Y133, E202, S203, W286, I294, F295, F297, Y341, H447, G448, I451	Y337, F338	W86	
4',5,7-Trimethoxyflavone **(5)**	-8.5	Y124, S203	D74, N87, G121, G122, S125, Y133, E202, S293, F295, R296, F297, Y341, H447, G448, I451	Y337, F338	W96, I294	

Luteolin **(6)**	-9.2	G122, S203, S293, Y337	W86, G120, G121, A204, W286, I294, F295, R296, F338, H447	Y124, F297, Y341	-	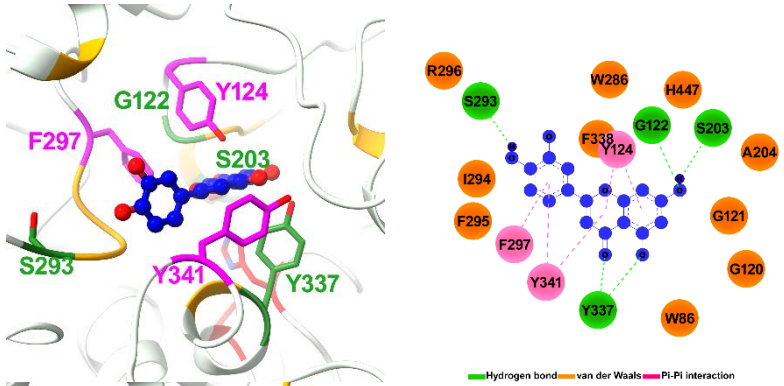
Epicatechin **(7)**	-8.0	Y124, S293	Y72, D74, L289, E291, E292, I294, F295, F297, Y337, F338	W286, Y341	-	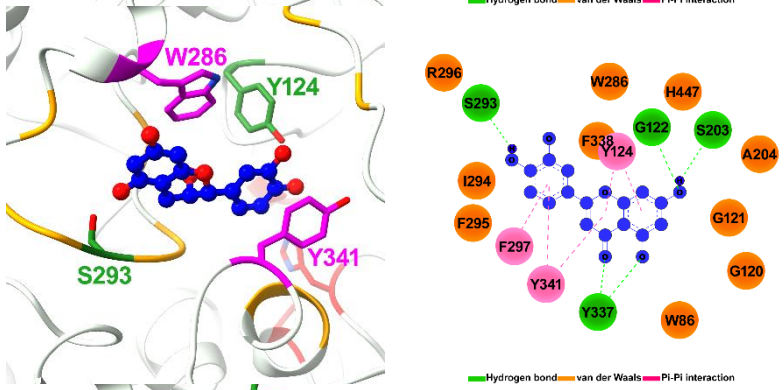
Galantamine	-7.8	Y72	D74, L76, Y124, L289, S293, I294, F295, R296, F297, Y337, F338, G342	W286, Y341	-	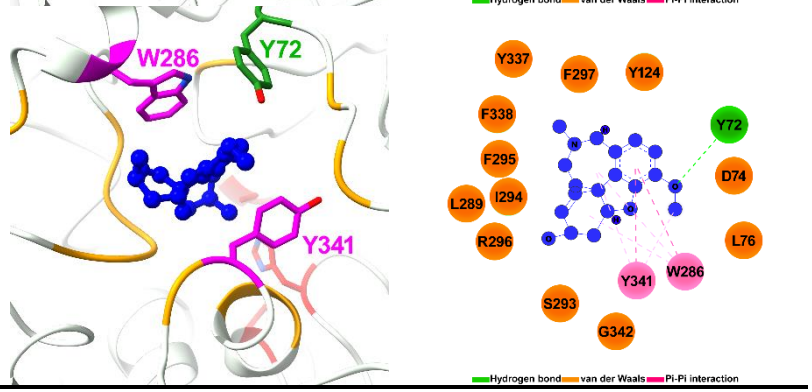

These interactions were further analyzed by identifying key hydrogen bonds, van der Waals forces, π-π stacking, and π-alkyl interactions within the active site of AChE. A peripheral anionic binding site (PAS) was identified near the entrance of the active site gorge. The active site of AChE consists of an esteratic site (ES) at the base of the gorge, which harbours the catalytic triad, an oxyanion hole (OAH) that stabilizes the tetrahedral intermediate during the interaction with the carbamate carbonyl group, and an acyl binding site (ABS) that accommodates the acetyl group of acetylcholine (ACh) or potentially the alkyl group of alternative inhibitors [37]. To inhibit enzyme activity, low binding energy is required to activate the protein-ligand interaction, which results in tightening the enzyme-inhibitor complexation pocket [38].

Among the tested compounds, cubebin acetate **(2)** exhibited the most favorable binding energy (-10.2 kcal/mol), followed by bicubebin A **(3)** (-10.0 kcal/mol) and aptosimon **(1)** (-9.4 kcal/mol). These three compounds demonstrated strong interactions within the active site of AChE, forming extensive van der Waals interactions and hydrogen bonding with key catalytic residues such as F295, G121, S125, and Y124. Notably, aptosimon **(1)** also engaged in π-π stacking interactions with Y124 and Y342, which may contribute to its stable binding. Interestingly, the in vitro AChE inhibition results revealed that aptosimon **(1)** exhibited the highest inhibitory activity (IC_{50} = 60.8 μM), even though its docking score was slightly lower than that of cubebin acetate **(2)** and bicubebin A **(3)**. This suggests that while docking scores provide insight into binding affinity, additional factors such as solubility, bioavailability, and molecular flexibility may influence the inhibitory potential. The strong in vitro activity of aptosimon **(1)** could be attributed to its optimal interaction within the active site, allowing effective inhibition of AChE function.

The flavonoid derivatives, including 5,7-dimethoxyflavone **(4)**, 4',5,7-trimethoxyflavone **(5)**, luteolin **(6)**, and epicatechin **(7)**, exhibited moderate docking scores (-8.0 to -9.2 kcal/mol). Their interactions were characterized by hydrogen bonding with key catalytic residues and π-π stacking with aromatic residues (F297, Y341, Y337). The methoxy (-OCH_3) groups in flavones 4 and 5 contributed to hydrophobic interactions, while hydroxyl (-OH) groups in luteolin and epicatechin facilitated additional hydrogen bonding, which may enhance binding stability. These docking results correlate well with the in vitro AChE inhibition data, particularly for aptosimon **(1)**, which exhibited strong binding affinity and enzyme inhibition. These findings highlight the potential of these compounds as promising AChE inhibitors, warranting further investigation.

In addition to that, Toxicity prediction was conducted using the ProTox 3.0 platform. As described in [31], the platform employs molecular similarity, pharmacophore analysis, fragment propensity assessments, and machine learning models to predict a wide array of toxicity endpoints. These include acute oral toxicity (reported as predicted LD_{50} values), organ toxicities (such as hepatotoxicity), various toxic endpoints (carcinogenicity, immunotoxicity, mutagenicity, cytotoxicity), molecular initiating events (for example, acetylcholinesterase inhibition), and more. Each endpoint is reported with a confidence score and graphical output (radar or network plots) that facilitates an integrated understanding of a compound's safety profile.

When applied to the compounds under investigation, the ProTox 3.0 predictions reveal subtle yet essential differences driven by the molecular structure. Compounds like Aptosimon **(1)**, Cubebin acetate B **(2)**, and Bicubebin A **(3)**, stemming from lignan scaffolds tend to demonstrate moderate signals for carcinogenicity and strong signals for immunotoxicity. In contrast, natural flavonoids such as luteolin and epicatechin are uniformly predicted as non-hepatotoxic, non-mutagenic, and non-cytotoxic, though luteolin shows a moderate potential for carcinogenicity. Meanwhile, the

predictions for the flavonoid derivatives highlight the profound impact of minor structural modifications. The case of 5,7-dimethoxyflavone **(4)** shows a borderline active prediction for acetylcholinesterase inhibition alongside inactive predictions for most other toxicity endpoints.

For 4',5,7-trimethoxyflavone **(5)**, ProTox 3.0 still predicts a benign hepatotoxicity profile (with low probability for liver injury) and confirms a non-cytotoxic and non-immunotoxic behavior. However, like many methoxy-substituted flavonoids, its carcinogenicity endpoint reaches a borderline active status, suggesting that while overall safety may be high, there exists a moderate risk signal that warrants further experimental validation. Moreover, its AChE inhibition potential hovers near the borderline between active and inactive predictions. It underscores that even subtle modifications, such as adding an extra methoxy group, can impact key molecular interactions with biological targets. Table 4 shows the toxicity results of the compounds.

Table 4 Toxicity results of the isolated compounds.

Compound	Hepatotoxicity	Carcinogenicity	Immunotoxicity	Mutagenicity	Cytotoxicity	AChE Inhibition
Aptosimon (1)	Inactive (Prob. 0.78)	Active (Prob. 0.68)	Active (Prob. 0.92)	Inactive (Prob. 0.61)	Inactive (Prob. 0.88)	Inactive (Prob. 0.61)
Cubebin acetate (2)	Inactive (Prob. 0.82)	Active (Prob. 0.57)	Active (Prob. 0.96)	Inactive (Prob. 0.57)	Inactive (Prob. 0.98)	Inactive (Prob. 0.53)
Bicubebin A (3)	Inactive (Prob. 0.84)	Active (Prob. 0.63)	Active (Prob. 0.97)	Inactive (Prob. 0.60)	Inactive (Prob. 0.96)	Inactive (Prob. 0.56)
5,7-Dimethoxyflavone (4)	Inactive (Prob. 0.73)	Active (Prob. 0.56)	Inactive (Prob. 0.85)	Inactive (Prob. 0.51)	Inactive (Prob. 0.57)	Active (Prob. 0.50)
4′,5,7-Trimethoxyflavone (5)	Inactive (Prob. 0.72)	Active (Prob. 0.53)	Inactive (Prob. 0.67)	Active (Prob. 0.56)	Inactive (Prob. 0.52)	Inactive (Prob. 0.72)
Luteolin (6)	Inactive (Prob. 0.69)	Active (Prob. 0.68)	Inactive (Prob. 0.97)	Active (Prob. 0.51)	Inactive (Prob. 0.99)	Inactive (Prob. 0.69)
Epicatechin (7)	Inactive (Prob. 0.72)	Inactive (Prob. 0.51)	Inactive (Prob. 0.96)	Inactive (Prob. 0.55)	Inactive (Prob. 0.84)	Inactive (Prob. 0.72)

Collectively, the ProTox 3.0 predictions across the compound series highlight the sensitivity of in silico models to even subtle structural variations. Natural flavonoids, such as luteolin and epicatechin, were predicted to exhibit relatively benign toxicity profiles, with low probabilities for hepatotoxicity, mutagenicity, immunotoxicity, and cytotoxicity. In contrast, lignan derivatives and methoxy-substituted flavonoids, including aptosimon **(1)**, cubebin acetate **(2)**, bicubebin A **(3)**, 5,7-dimethoxyflavone **(4)**, and 4',5,7-trimethoxyflavone **(5)**, demonstrated signals for immunotoxicity and carcinogenicity, which warrant further experimental scrutiny.

4. Conclusions

In this study, seven bioactive compounds were successfully isolated from the leaf extract of *K. hookeriana*, including a furofuran lignan, two cubebin-type lignans, two methoxyflavones, a hydroxyflavone, and a flavonol. Among these, aptosimon **(1)** exhibited the most potent AChE inhibitory activity, highlighting its potential as a lead compound for neurodegenerative drug discovery. The molecular docking analysis further supported the in vitro findings, demonstrating strong binding interactions between the isolated compounds and AChE, particularly through hydrogen bonding, van der Waals forces, and π-π stacking interactions. The significant inhibitory activity observed for aptosimon **(1)**, cubebin acetate **(2)**, and bicubebin A **(3)** suggests that lignan derivatives from *K. hookeriana* could serve as promising candidates for acetylcholinesterase inhibition. These results underscore the potential of *Knema* species as a valuable source of bioactive natural products with neuroprotective properties. However, further studies, including molecular dynamics simulations and in vivo evaluations, are essential to confirm the stability, bioavailability, and therapeutic efficacy of these compounds. Future research should explore semi-synthetic modifications to improve pharmacokinetics and conduct thorough toxicological assessments to ensure safety. This study enhances the understanding of natural acetylcholinesterase inhibitors, supporting the development of new treatments for neurodegenerative diseases like Alzheimer's.

Acknowledgments

The authors would like to thank the Department of Chemistry, Faculty of Science and Mathematics, Universiti Pendidikan Sultan Idris, for research facilities. The authors would also like to thank Dr. Shamsul Khamis, Director of Fraser's Hill Research Center for plant identification.

Author Contributions

Abubakar Siddiq Salihu: Conceptualization, writing original draft and formal analysis. Wan Mohd Nuzul Hakimi Wan Salleh: Review and editing. Nurunajah Ab Ghani and Mohd Hafiz Arzmi: Methodology, review and editing. Bunleu Sungthong and Ravikumar Kapavarapu: Conceptualization. All authors have read and approved the published version of the manuscript.

Funding

This research was supported by the Geran Penyelidikan Universiti (Kecemerlangan@UPSI) under grant number 2025-0012-103-01, funded by Universiti Pendidikan Sultan Idris.

Competing Interests

The authors have declared that no competing interests exist.

References

1. Boy S, Türkan F, Beytur M, Aras A, Akyıldırım O, Karaman HS, et al. Synthesis, design, and assessment of novel morpholine-derived Mannich bases as multifunctional agents for the potential enzyme inhibitory properties including docking study. Bioorg Chem. 2021; 107: 104524.
2. Türkan F, Cetin A, Rozbicki P, Oğuz E, Wolińska E, Branowska D. Pharmacological assessment of disulfide-triazine hybrids: Synthesis, enzyme inhibition, and molecular docking study. Med Chem Res. 2024; 33: 1205-1217.
3. Colovic MB, Krstic DZ, Lazarevic-Pasti TD, Bondzic AM, Vasic VM. Acetylcholinesterase inhibitors: Pharmacology and toxicology. Curr Neuropharmacol. 2013; 11: 315-335.
4. Lane RM, Potkin SG, Enz A. Targeting acetylcholinesterase and butyrylcholinesterase in dementia. Int J Neuropsychopharmacol. 2006; 9: 101-124.
5. Zhang J, Zhang C, Xu FC, Zhang QY, Tu PF, Liang H. Cholinesterase inhibitory isoquinoline alkaloids from Corydalis mucronifera. Phytochemistry. 2019; 159: 199-207.
6. Minocha T, Birla H, Obaid AA, Rai V, Sushma P, Shivamallu C, et al. Flavonoids as promising neuroprotectants and their therapeutic potential against Alzheimer's disease. Oxid Med Cell Longev. 2022; 2022: 6038996.
7. Zálešák F, Bon DJ, Pospíšil J. Lignans and neolignans: Plant secondary metabolites as a reservoir of biologically active substances. Pharmacol Res. 2019; 146: 104284.
8. Jabir NR, Khan FR, Tabrez S. Cholinesterase targeting by polyphenols: A therapeutic approach for the treatment of Alzheimer's disease. CNS Neurosci Ther. 2018; 24: 753-762.
9. Azmal M, Hossen MS, Shohan MN, Taqui R, Malik A, Ghosh A. A computational approach to identify phytochemicals as potential inhibitor of acetylcholinesterase: Molecular docking, ADME profiling and molecular dynamics simulations. PLoS One. 2024; 19: e0304490.
10. Burkill IH. A dictionary of the economic products of the Malay Peninsula. Kuala Lumpur, Malaysia: Ministry of Agriculture and Co-operatives; 1966.
11. Geny C, Rivière G, Bignon J, Birlirakis N, Guittet E, Awang K, et al. Anacardic acids from Knema hookeriana as modulators of Bcl-xL/Bak and Mcl-1/Bid interactions. J Nat Prod. 2016; 79: 838-844.
12. Alen Y, Nakajima S, Nitoda T, Baba N, Kanzaki H, Kawazu K. Antinematodal activity of some tropical rainforest plants against the pinewood nematode, Bursaphelenchus xylophilus. Z Naturforsch C. 2000; 55: 295-299.
13. Salihu AS, Salleh WM, Ogunwa TH. Chemical composition, acetylcholinesterase inhibition and molecular docking studies of essential oil from Knema hookeriana Warb. (Myristicaceae). Nat Prod Res. 2024; 38: 2516-2521.
14. Lee MY, Park BY, Kwon OK, Yuk JE, Oh SR, Kim HS, et al. Anti-inflammatory activity of (−)-aptosimon isolated from Daphne genkwa in RAW264. 7 cells. Int Immunopharmacol. 2009; 9: 878-885.

15. Conrado GG, Grazzia N, Adriana da Silva S, Franco CH, Moraes CB, Gadelha FR, et al. Prospecting and identifying Phyllanthus Amarus lignans with antileishmanial and antitrypanosomal activity. Planta Med. 2020; 86: 782-789.
16. Davidson SJ, Pearce AN, Copp BR, Barker D. Total synthesis of (−)-bicubebin A, B, (+)-bicubebin C and structural reassignment of (−)-cis-cubebin. Org Lett. 2017; 19: 5368-5371.
17. Rezod UJ, Salleh WM, Salihu NA, Sungthong B. Antioxidant constituents from the leaves of piper crassipes Korth ex Miq. growing in Malaysia. Bull Chem Soc Ethiop. 2025; 39: 561-570.
18. Salleh WM, Nafiah MA, Yen KH, Kassim H, Tawang A. Chemical constituents and acetylcholinesterase inhibitory activity of piper abbreviatum Opiz. Bull Chem Soc Ethiop. 2020; 34: 625-632.
19. Ueda H, Yamazaki C, Yamazaki M. Luteolin as an anti-inflammatory and anti-allergic constituent of Perilla frutescens. Biol Pharm Bull. 2002; 25: 1197-1202.
20. Sheehan EW, Zemaitis MA, Slatkin DJ, Schiff Jr PL. A constituent of Pterocarpus marsupium, (−)-epicatechin, as a potential antidiabetic agent. J Nat Prod. 1983; 46: 232-234.
21. Ellman GL, Courtney KD, Andres Jr V, Featherstone RM. A new and rapid colorimetric determination of acetylcholinesterase activity. Biochem Pharmacol. 1961; 7: 88-95.
22. Salleh WM, Ahmad F, Khong HY. Chemical composition of piper stylosum Miq. and piper ribesioides Wall. essential oils, and their antioxidant, antimicrobial and tyrosinase inhibition activities. Bol Latinoam Caribe Plantas Med Aromat. 2014; 13: 488-497.
23. Salleh WM, Ahmad F, Yen KH, Sirat HM. Chemical compositions, antioxidant and antimicrobial activity of the essential oils of piper officinarum (Piperaceae). Nat Prod Commun. 2012; 7. doi: 10.1177/1934578X1200701229.
24. Bourne Y, Grassi J, Bougis PE, Marchot P. Conformational flexibility of the acetylcholinesterase tetramer suggested by x-ray crystallography. J Biol Chem. 1999; 274: 30370-30376.
25. Dassault Systèmes. BIOVIA Materials Studio [Internet]. Paris, France: Dassault Systèmes; 2025. Available from: https://www.3ds.com/products/biovia/materials-studio.
26. Imramovsky A, Stepankova S, Vanco J, Pauk K, Monreal-Ferriz J, Vinsova J, et al. Acetylcholinesterase-inhibiting activity of salicylanilide N-alkylcarbamates and their molecular docking. Molecules. 2012; 17: 10142-10158.
27. Frisch MJ, Trucks GW, Schlegel HB, Scuseria GE, Robb MA, Cheeseman JR, et al. Gaussian 03. Revision C.02 [Internet]. Berlin, Germany: ScienceOpen, Inc.; 2003. Available from: https://www.scienceopen.com/document?vid=c6dcfe99-1f71-437a-b4ed-ab662a8383f3.
28. Morris GM, Huey R, Lindstrom W, Sanner MF, Belew RK, Goodsell DS, et al. AutoDock4 and AutoDockTools4: Automated docking with selective receptor flexibility. J Comput Chem. 2009; 30: 2785-2791.
29. Sungthong B, Sithon K, Panyatip P, Tadtong S, Nunthaboot N, Puthongking P. Quantitative analysis and in silico molecular docking screening for acetylcholinesterase inhibitor and ADME prediction of coumarins and carbazole alkaloids from Clausena harmandiana. Rec Nat Prod. 2022; 16: 358-369.
30. Pettersen EF, Goddard TD, Huang CC, Couch GS, Greenblatt DM, Meng EC, et al. UCSF chimera-a visualization system for exploratory research and analysis. J Comput Chem. 2004; 25: 1605-1612.
31. Banerjee P, Kemmler E, Dunkel M, Preissner R. ProTox 3.0: A webserver for the prediction of toxicity of chemicals. Nucleic Acids Res. 2024; 52: W513-W520.

32. Yamauchi S, Yamaguchi M. Synthesis of (+)-aptosimon, a 4-oxofurofuran lignan, by erythro selective aldol condensation and stereoconvergent cyclization as the key reactions. Biosci Biotechnol Biochem. 2003; 67: 838-846.
33. Rezende K, Lucarini R, Símaro GV, Pauletti PM, Januário AH, Esperandim VR, et al. Antibacterial activity of (−)-cubebin isolated from piper cubeba and its semisynthetic derivatives against microorganisms that cause endodontic infections. Rev Bras Farmacogn. 2016; 26: 296-303.
34. Shakri NM, Salleh WM, Khamis S. Chemical constituents of polyalthia rumphii. Chem Nat Compd. 2021; 57: 1114-1115.
35. Salleh WM, Ahmad F, Yen KH. Chemical constituents from piper caninum and antibacterial activity. J Appl Pharm Sci. 2015; 5: 20-25.
36. Ismail N, Akhtar MN, Ismail M, Zareen S, Shah SA, Lajis NH, et al. Neuroprotective effect from stem bark extracts of Knema laurina against H_2O_2-and $A\beta_{1-42}$-induced cell death in human SH-SY5Y cells. Nat Prod Res. 2015; 29: 1571-1574.
37. Yılmaz C, Khorsheed WM, Babat CF. *In vitro* and *in silico* evaluation of inhibitory effects of bisphenol derivatives on acetylcholinesterase of electric eel (*Electrophorus electricus* L.). Comp Biochem Physiol C Toxicol Pharmacol. 2022; 260: 109416.
38. Sajid A, Sajid A, Ahmed E, Sharif A, Manzoor Q, Al-Mijalli SH, et al. *In-vitro* and molecular docking studies of plant secondary metabolites isolated from *Hypericum oblongifolium* as antibacterial agents and lipoxygenase (5-LOX) inhibitors. J Mol Struct. 2024; 1312: 138549.